Dichotomy of Electron-Phonon Coupling in Graphene Moiré Flat Bands

Young Woo Choi and Hyoung Joon Choi*
Department of Physics, Yonsei University, Seoul 03722, Korea

(Received 8 April 2021; accepted 3 September 2021; published 11 October 2021)

Graphene moiré superlattices are outstanding platforms to study correlated electron physics and superconductivity with exceptional tunability. However, robust superconductivity has been measured only in magic-angle twisted bilayer graphene (MA-TBG) and magic-angle twisted trilayer graphene (MA-TTG). The absence of a superconducting phase in certain moiré flat bands raises a question on the superconducting mechanism. In this work, we investigate electronic structure and electron-phonon coupling in graphene moiré superlattices based on atomistic calculations. We show that electron-phonon coupling strength λ is dramatically different among graphene moiré flat bands. The total strength λ is very large ($\lambda > 1$) for MA-TBG and MA-TTG, both of which display robust superconductivity in experiments. However, λ is an order of magnitude smaller in twisted double bilayer graphene (TDBG) and twisted monolayer-bilayer graphene (TMBG) where superconductivity is reportedly rather weak or absent. We find that the Bernal-stacked layers in TDBG and TMBG induce sublattice polarization in the flat-band states, suppressing intersublattice electron-phonon matrix elements. We also obtain the nonadiabatic superconducting transition temperature T_c that matches well with the experimental results. Our results clearly show a correlation between strong electron-phonon coupling and experimental observations of robust superconductivity.

DOI: 10.1103/PhysRevLett.127.167001

Moiré materials have emerged as precisely tunable platforms to explore fascinating physical phenomena [1]. For example, twisted bilayer graphene (TBG) was predicted to have nearly flat bands at certain "magic angles" (MAs) [2–5], and experimentally shown to host correlated insulators and superconductivity [6,7]. Subsequently, various interaction-driven phases have been realized not only in magic-angle twisted bilayer graphene (MA-TBG) [8–13] but also in other graphene moiré superlattices [14–20]. In addition to electronic properties, extensive aspects of moiré physics have been actively explored, such as moiré excitons [21,22] and atomic-structure and phonon reconstructions [23–25].

While correlated insulating states are observed in many graphene moiré superlattices having flat bands, MA-TBG has been the only system to show robust superconductivity until recent experiments added magic-angle alternating-twist trilayer graphene (TTG) to the list [7,18,19]. In other systems, such as twisted double bilayer graphene (TDBG) and twisted monolayer-bilayer graphene (TMBG), superconducting phase appears to be rather weak or absent [15,16,26].

Naturally, the absence of robust superconductivity in some graphene moiré flat bands raises more questions on the superconducting mechanism. In particular, theoretical studies on MA-TBG have suggested that MA-TBG has strong electron-phonon coupling and phonon-mediated superconductivity is a strong candidate [27–30]. Also, strong electron-phonon coupling in MA-TBG is evidenced in experiments [25,31]. However, whether all the flat-band states in graphene moiré superlattices have such strong electron-phonon coupling is still unanswered, which has an important implication for the superconducting mechanism.

In this work, we investigate electronic structure and electron-phonon coupling of graphene moiré superlattices based on atomistic calculations. We show that electron-phonon coupling is strong ($\lambda > 1$) for TBG and TTG at their magic angles, but it is an order of magnitude weaker for TDBG and TMBG. We analyze such difference in λ in terms of both density of states and matrix-element effects. We find that Bernal-stacked layers in TDBG and TMBG induce sublattice polarization in flat-band states, suppressing intersublattice electron-phonon matrix elements. Regardless of the total coupling strength, characteristic phonon modes are the same for all systems. We also calculate effects of vertical electric fields on electronic structure and electron-phonon coupling. Our calculations show that a correlation exists between strong electron-phonon coupling and experimental observations of robust superconductivity.

We consider four graphene moiré superlattices at their respective magic angle, which is defined by the angle of the minimum bandwidth: TBG with $\theta = 1.08°$, TTG with an alternating twist angle $\theta = 1.61°$, TDBG with $\theta = 1.35°$, and TMBG with $\theta = 1.25°$. TBG consists of two graphene layers with a twist, TTG is a three-layer system where only the middle layer is twisted, TDBG has two sets of Bernal-stacked bilayer graphene with a twist between them, and

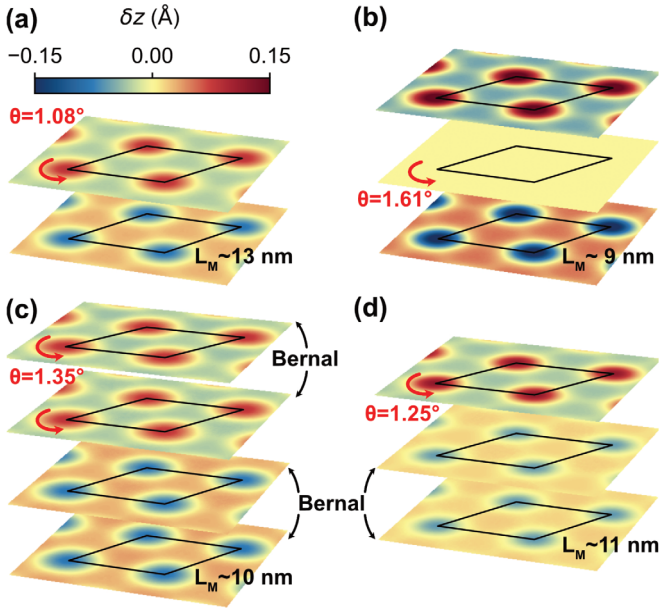

FIG. 1. Atomic relaxation patterns of (a) TBG with $\theta = 1.08°$, (b) TTG with an alternating twist angle $\theta = 1.61°$, (c) TDBG with $\theta = 1.35°$, and (d) TMBG with $\theta = 1.25°$. δz is the deviation of atomic positions in the out-of-plane direction from the average value within each layer. Topmost two layers in (c) and bottom two layers in (c) and (d) are Bernal-stacked without twist.

TMBG is built by twisting a monolayer on the top of Bernal-stacked bilayer graphene.

We adopt atomistic approaches to calculate electrons and phonons in graphene moiré superlattices [28]. First, we calculate structural relaxations induced by variation of the stacking registry within moiré supercells, which have crucial effects on electronic structure of moiré flat bands [23,32]. Equilibrium positions of all the carbon atoms are obtained by minimizing the sum of in-plane elastic energy and interlayer van der Waals binding energy [33,34]. Then, electron states are obtained by diagonalizing atomistic tight-binding Hamiltonians with the Slater-Koster-type hopping integral parameterized for graphitic systems [35,36]. We calculate all the phonon modes in moiré supercells by diagonalizing dynamical matrices built from atomic force constants, which are the second derivatives of our total-energy function. With electron and phonon eigenstates, we compute electron-phonon matrix elements from changes in hopping amplitudes due to atomic displacements of phonon modes. From the above quantities, we can obtain electron-phonon coupling strength λ and the Eliashberg function $\alpha^2F(\omega)$ (See the Supplemental Material [37] for detailed descriptions of our methods).

Figure 1 shows our results of atomic relaxation patterns. δz is the deviation of atomic positions in the out-of-plane direction from the average value of each layer. The average interlayer distances are about 3.40 Å between twisted layers and 3.35 Å between Bernal-stacked layers in TDBG and TMBG. In all systems, δz is largest at AA stacking regions and has the opposite sign between twisted layers, except for TTG where the middle layer has zero δz due to the symmetry and the other layers have large δz in compensation. In our calculation, in-plane relaxations also occur in such a way to reduce the area of AA-stacked regions.

Figure 2(a) shows our calculated band structures and density of states (DOS) per spin. All the four systems have

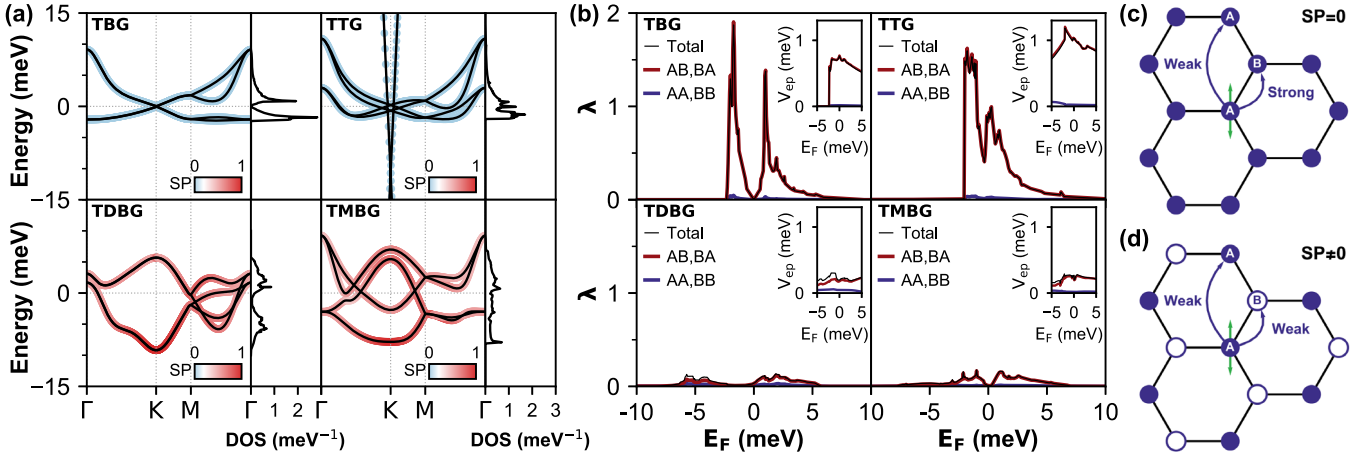

FIG. 2. (a) Band structure and density of states (DOS) per spin and (b) electron-phonon coupling strength λ as a function of the Fermi energies E_F in (upper left) TBG with $\theta = 1.08°$, (upper right) TTG with $\theta = 1.61°$, (lower left) TDBG with $\theta = 1.35°$, and (lower right) TMBG with $\theta = 1.25°$. In (a), colored circles represent sublattice polarization (SP). TBG and TTG have exactly zero sublattice polarization. In (b), black lines show the total coupling strength. Red (blue) lines represent contributions of the inter- (intra-) sublattice electron-phonon coupling. In each case, the inset shows the average electron-phonon matrix element $V_{ep} = \lambda/N_F$, where N_F is the DOS per spin at E_F. (c),(d) Illustrations of how sublattice polarization suppresses intersublattice electron-phonon matrix elements. Blue arrows indicate electron-phonon matrix elements induced by phonon displacements denoted by green arrows. When sublattice polarization is nonzero in (d), the nearest-neighbor electron-phonon matrix elements are weakened.

nearly flat bands and large DOS at their Fermi levels. Flat bands in TBG are the most archetypical in that nearly flat Dirac cones are located at the corners of the moiré Brillouin zone and isolated from the higher-energy bands. In TTG, the highly dispersing Dirac cone coexists with moiré flat bands. It comes from the outer graphene layers and is decoupled from the flat bands. In TDBG and TMBG, Dirac points at K points are gapped because the absence of the inversion symmetry brings sublattice asymmetry. Our electronic structures are consistent with previous theoretical studies [28,41–44].

While TBG, TTG, TDBG, and TMBG at their respective magic angle have flat bands and large DOS at the Fermi level, we find a clear distinction of electron-phonon coupling strength λ between the first two and last two systems. Figure 2(b) shows the total electron-phonon coupling strength of each system as a function of the Fermi energy. The most notable feature is that λ is very strong in TBG and TTG with the maximum value reaching over 1, but it is an order of magnitude weaker in TDBG and TMBG. For TDBG and TMBG, λ is less than 0.2 irrespective of the Fermi energy.

Such stark contrast in λ originates partly from the difference in the electronic density of states, but more crucially from the suppression of electron-phonon matrix elements in TDBG and TMBG. Insets in Fig. 2(b) show the average of electron-phonon matrix elements $V_{\rm ep} = \lambda/N_F$, where N_F is the electronic density of states at the Fermi energy E_F. While $V_{\rm ep}$ in TBG and TTG is about 0.75 and 1.0 meV, respectively, it is below 0.3 meV in TDBG and TMBG.

To explain why $V_{\rm ep}$ is suppressed in TDBG and TMBG, we introduce sublattice polarization (SP) which measures the imbalance of sublattice weights of an electron state. For a given electron state $\psi_{n\mathbf{k}}$, we define SP for each layer l as

$$\mathrm{SP}_l(\psi_{n\mathbf{k}}) = \sum_{i\in A}|c_{n\mathbf{k},i}|^2 - \sum_{j\in B}|c_{n\mathbf{k},j}|^2, \qquad (1)$$

where $c_{n\mathbf{k},i}$ is the tight-binding coefficient of $\psi_{n\mathbf{k}}$ for an orbital centered at an atomic site i and A, B indicate two different sublattices. Then, the total SP, which is represented by colored circles in Fig. 2(a), is $\mathrm{SP}(\psi_{n\mathbf{k}}) = \sum_l |\mathrm{SP}_l(\psi_{n\mathbf{k}})|$. In TBG and TTG, the SP is exactly zero for all the electron states so they have the equal weights on two sublattices. In contrast, TDBG and TMBG, which both have Bernal-stacked layers, have nonzero SP and electrons have different sublattice weights within each layer, with signs of SP_l alternating for different layers.

The presence of nonzero SP in the electronic structure of TDBG and TMBG critically weakens electron-phonon coupling strength. To illustrate this, we analyze the total electron-phonon coupling strength in terms of sublattice-dependent contributions. Figure 2(b) shows the total electron-phonon coupling strength λ, and intersublattice ($\lambda^{AB} + \lambda^{BA}$) and intrasublattice ($\lambda^{AA} + \lambda^{BB}$) contributions as a function of the Fermi energy (see the Supplemental Material [37] for the formulas for inter- and intrasublattice λ). We find that, in all cases, the magnitude of the intersublattice contributions dominates the total coupling strength. This is because the strongest contribution comes from the electron-phonon matrix elements between the nearest neighbors, which belong to different sublattices [Fig. 2(c)]. In TBG and TTG, where SP is zero, electron wave functions have the same weights on both sublattices and the intersublattice matrix elements are strong. On the other hand, in TDBG and TMBG, nonzero SP suppresses the nearest-neighbor matrix elements [Fig. 2(c)], and the electron-phonon coupling becomes very weak.

Now, we analyze characteristic phonon modes that contribute to the total coupling strength. Figure 3(a) shows the Eliashberg functions $\alpha^2F(\omega)$ and frequency-integrated electron-phonon coupling strength $\lambda(\omega) = 2\int_0^\omega \alpha^2F(\omega')/\omega' d\omega'$ of TBG and TTG (TDBG and TMBG) at the half-filling energy of the hole- (electron-) side. Regardless of the total coupling strength, characteristic phonon modes are the same for all systems. The largest portion of the total coupling strength comes from the in-plane optical modes near $\omega =$ 167 (197) meV with phonon momentums at $\mathbf{q} = \mathbf{K}, \mathbf{K}'$ ($\mathbf{\Gamma}$). In addition, the interlayer breathing modes near $\omega =$ 10 meV, shown in the insets of Fig. 3(a), at $\mathbf{q} = \mathbf{\Gamma}$ also

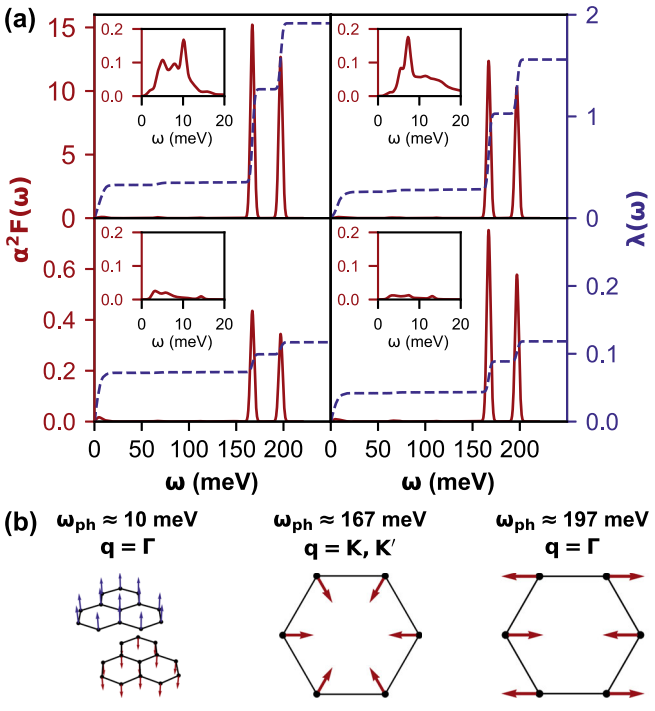

FIG. 3. (a) Eliashberg function $\alpha^2F(\omega)$, shown in red, at the half-filling energy of the hole-side in (upper left) TBG and (upper right) TTG, and the electron-side in (lower left) TDBG and (lower right) TMBG. Dashed blue lines denote frequency-integrated electron-phonon coupling strength $\lambda(\omega) = 2\int_0^\omega \alpha^2F(\omega')/\omega' d\omega'$. Insets show low-frequency ranges of $\alpha^2F(\omega)$. (b) Phonon frequencies and momenta of the characteristic modes.

TABLE I. Mode-resolved electron-phonon coupling strength λ_i, half bandwidth D, and nonadiabatic superconducting transition temperature T_c at the half-filling Fermi energy of the hole- (electron-) side flat bands for TBG and TTG (TDBG and TMBG). The half bandwidths are calculated as the difference between the Fermi energy and the band edge. μ is the dimensionless Coulomb potential.

	λ_i			
ω_i (meV)	TBG	TTG	TDBG	TMBG
10	0.297	0.233	0.064	0.037
167	0.914	0.743	0.026	0.045
197	0.648	0.532	0.018	0.030
D (meV)	0.53	0.67	3.4	6.7
$T_c(\mu = 0.05)$ (K)	3.45	3.76	10^{-7}	10^{-6}
$T_c(\mu = 0.15)$ (K)	3.33	3.55	0.0	0.0

have sizable contribution due to their low energies. Table I summarizes mode-resolved electron-phonon coupling strength λ_i for the three characteristic phonon modes shown in Fig. 3(b).

Since $E_F \approx 1$–10 meV and $\omega_{\mathrm{ph}} \approx 10$–$200$ meV, the adiabatic condition $\omega_{\mathrm{ph}}/E_F \ll 1$ is extremely violated in graphene moiré superlattices. So the conventional McMillan formula does not apply. Instead, superconducting transition temperature T_c in the nonadiabatic regime has nontrivial dependence on the electronic bandwidth [45,46]. If we ignore the dispersion of phonon modes and the energy dependence of the electron DOS, an explicit T_c formula for the half-filled bands can be derived as [46]

$$T_c = \prod_i \left(\frac{\omega_i D}{\omega_i + D}\right)^{\lambda_i/\lambda} \exp\left(-\frac{1+\tilde{\lambda}}{\lambda - \mu^*}\right), \qquad (2)$$

where D is the half bandwidth, ω_i and λ_i are the energy and electron-phonon coupling strength of the ith phonon mode, $\tilde{\lambda} = 2\sum_i \lambda_i D/(\omega_i + D)$ is the mass renormalization constant, and $\mu^* = \mu/(1 + \mu \sum_i \ln(1 + D/\omega_i)^{\lambda_i/\lambda})$ is the Coulomb pseudopotential. We calculate T_c at the half-filling Fermi energy of the hole- (electron-) side flat bands for TBG and TTG (TDBG and TMBG). Our results for T_c are summarized in Table I, and show good agreement with experimental observations in TBG and TTG [7,18,19].

Lastly, we investigate electric-field effects on electronic structure and electron-phonon coupling. We consider a vertical electric field in our tight-binding Hamiltonian by adding an electrostatic energy term $\Delta H = eE_z z$, where $e > 0$ is the elementary charge, z is the z coordinate of an atom, and E_z represents the total electric field consisting of external and induced electric fields.

Figures 4(a) and 4(b) show electronic structures and electron-phonon coupling strengths under the vertical electric field, respectively. In our calculation, TBG is nearly insensitive to the vertical electric field, except that

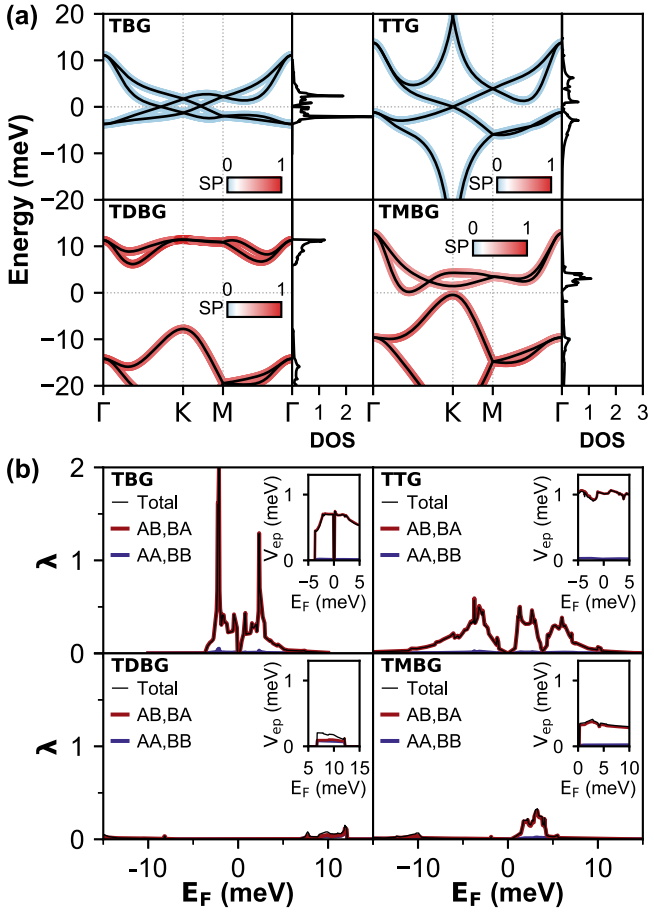

FIG. 4. (a) Electronic structure and (b) electron-phonon coupling in (upper left) TBG with $\theta = 1.08°$, (upper right) TTG with $\theta = 1.61°$, (lower left) TDBG with $\theta = 1.35°$, and (lower right) TMBG with $\theta = 1.25°$ under vertical electric field. The strength of electric field E_z is 15 (5) mV/Å for TBG and TTG (TDBG and TMBG). The unit of DOS in (a) is states/spin/meV. In (a), colors of band lines represent the sublattice polarization. TBG and TTG have exactly zero sublattice polarization. In (b), black lines show the total coupling strength. Red (blue) lines represent contributions of inter- (intra-) sublattice electron-phonon couplings.

two Dirac points at K are split in energy because of the potential energy difference between two layers. Consequently, electron-phonon coupling strength is hardly affected by the electric field. In TTG, the electric field primarily affects highly dispersive monolayer Dirac bands so that they are pushed away from the flat bands. This makes the flat-band states more dispersive, reducing the density of states and, accordingly, decreasing the electron-phonon coupling strength. However, V_{ep} is not affected by electric fields.

On the other hand, the electronic structures in TDBG and TMBG are much more sensitive to electric fields. In both systems, flat bands are split into the electron and hole sides, and the electron-side flat bands become narrower. Nevertheless, TDBG under electric fields shows very weak

λ because the sublattice polarization still suppresses V_{ep}. In more detail, we note a slight increase of λ in the electron-side flat bands of TMBG as the electric field polarizes the electron-side states to the top monolayer where sublattice polarization is weaker.

In TBG and TTG, superconductivity often appears near spin-valley flavor-polarized correlated phases at certain integer fillings [12,13,18,19,47]. Several studies have suggested that such correlated phases compete with the superconductivity [48,49]. In particular, experiments with controlled metallic gates have shown that superconductivity survives even after correlated phases disappear as a result of the enhanced screening from metallic gates [50]. Flavor polarization, if any, may weaken phonon-mediated superconductivity in two ways. First, flavor polarization may raise or lower band energies depending on their flavors, increasing the band width and reducing the density of states, which reduces the overall electron-phonon coupling strength. Second, flavor polarization may lift energy degeneracy of electron states with opposite momenta and opposite spins, for instance, $|\mathbf{k},\uparrow\rangle$ and $|-\mathbf{k},\downarrow\rangle$, which disturbs Cooper-pair formation for spin-singlet superconductivity. Effects of flavor polarization and electron correlation need to be studied for a full phase diagram of twisted graphene layers. In addition, further studies should include doping-dependent band dispersions and more accurate description of Coulomb matrix elements [51–55].

To summarize, we have studied electronic structure and electron-phonon coupling in graphene moiré superlattices based on atomistic approaches. We find that total electron-phonon coupling is strong for MA-TBG and MA-TTG, but is an order of magnitude weaker for TDBG and TMBG, where the Bernal-stacked layers induce sublattice polarization, suppressing the nearest-neighbor electron-phonon matrix elements. Our results provide a deeper understanding into the electron-phonon coupling in graphene moiré superlattices, showing a correlation between strong electron-phonon coupling and experimental observations of robust superconductivity.

This work was supported by NRF of Korea (Grants No. 2020R1A2C3013673 and No. 2017R1A5A1014862) and KISTI supercomputing center (Project No. KSC-2020-CRE-0335). Y. W. C. acknowledges support from NRF of Korea (Global Ph.D. Fellowship Program NRF-2017H1A2A1042152).

*h.j.choi@yonsei.ac.kr

[1] E. Y. Andrei, D. K. Efetov, P. Jarillo-Herrero, A. H. MacDonald, K. F. Mak, T. Senthil, E. Tutuc, A. Yazdani, and A. F. Young, The marvels of moiré materials, Nat. Rev. Mater. **6**, 201 (2021).

[2] R. Bistritzer and A. H. MacDonald, Moiré bands in twisted double-layer graphene, Proc. Natl. Acad. Sci. U.S.A. **108**, 12233 (2011).

[3] J. M. B. Lopes dos Santos, N. M. R. Peres, and A. H. Castro Neto, Graphene Bilayer with a Twist: Electronic Structure, Phys. Rev. Lett. **99**, 256802 (2007).

[4] S. Shallcross, S. Sharma, E. Kandelaki, and O. A. Pankratov, Electronic structure of turbostratic graphene, Phys. Rev. B **81**, 165105 (2010).

[5] E. Suárez Morell, J. D. Correa, P. Vargas, M. Pacheco, and Z. Barticevic, Flat bands in slightly twisted bilayer graphene: Tight-binding calculations, Phys. Rev. B **82**, 121407 (R) (2010).

[6] Y. Cao, V. Fatemi, A. Demir, S. Fang, S. L. Tomarken, J. Y. Luo, J. D. Sanchez-Yamagishi, K. Watanabe, T. Taniguchi, E. Kaxiras, R. C. Ashoori, and P. Jarillo-Herrero, Correlated insulator behaviour at half-filling in magic-angle graphene superlattices, Nature (London) **556**, 80 (2018).

[7] Y. Cao, V. Fatemi, S. Fang, K. Watanabe, T. Taniguchi, E. Kaxiras, and P. Jarillo-Herrero, Unconventional superconductivity in magic-angle graphene superlattices, Nature (London) **556**, 43 (2018).

[8] Y. Choi, H. Kim, Y. Peng, A. Thomson, C. Lewandowski, R. Polski, Y. Zhang, H. S. Arora, K. Watanabe, T. Taniguchi, J. Alicea, and S. Nadj-Perge, Correlation-driven topological phases in magic-angle twisted bilayer graphene, Nature (London) **589**, 536 (2021).

[9] K. P. Nuckolls, M. Oh, D. Wong, B. Lian, K. Watanabe, T. Taniguchi, B. A. Bernevig, and A. Yazdani, Strongly correlated Chern insulators in magic-angle twisted bilayer graphene, Nature (London) **588**, 610 (2020).

[10] H. Polshyn, J. Zhu, M. A. Kumar, Y. Zhang, F. Yang, C. L. Tschirhart, M. Serlin, K. Watanabe, T. Taniguchi, A. H. MacDonald, and A. F. Young, Electrical switching of magnetic order in an orbital Chern insulator, Nature (London) **588**, 66 (2020).

[11] M. Serlin, C. L. Tschirhart, H. Polshyn, Y. Zhang, J. Zhu, K. Watanabe, T. Taniguchi, L. Balents, and A. F. Young, Intrinsic quantized anomalous Hall effect in a moiré heterostructure, Science **367**, 900 (2020).

[12] D. Wong, K. P. Nuckolls, M. Oh, B. Lian, Y. Xie, S. Jeon, K. Watanabe, T. Taniguchi, B. A. Bernevig, and A. Yazdani, Cascade of electronic transitions in magic-angle twisted bilayer graphene, Nature (London) **582**, 198 (2020).

[13] U. Zondiner, A. Rozen, D. Rodan-Legrain, Y. Cao, R. Queiroz, T. Taniguchi, K. Watanabe, Y. Oreg, F. von Oppen, A. Stern, E. Berg, P. Jarillo-Herrero, and S. Ilani, Cascade of phase transitions and Dirac revivals in magic-angle graphene, Nature (London) **582**, 203 (2020).

[14] G. Chen, A. L. Sharpe, P. Gallagher, I. T. Rosen, E. J. Fox, L. Jiang, B. Lyu, H. Li, K. Watanabe, T. Taniguchi, J. Jung, Z. Shi, D. Goldhaber-Gordon, Y. Zhang, and F. Wang, Signatures of tunable superconductivity in a trilayer graphene moiré superlattice, Nature (London) **572**, 215 (2019).

[15] X. Liu, Z. Hao, E. Khalaf, J. Y. Lee, Y. Ronen, H. Yoo, D. H. Najafabadi, K. Watanabe, T. Taniguchi, A. Vishwanath, and P. Kim, Tunable spin-polarized correlated states in twisted double bilayer graphene, Nature (London) **583**, 221 (2020).

[16] Y. Cao, D. Rodan-Legrain, O. Rubies-Bigorda, J. M. Park, K. Watanabe, T. Taniguchi, and P. Jarillo-Herrero, Tunable correlated states and spin-polarized phases in twisted bilayer–bilayer graphene, Nature (London) **583**, 215 (2020).

[17] G. Chen, A. L. Sharpe, E. J. Fox, Y.-H. Zhang, S. Wang, L. Jiang, B. Lyu, H. Li, K. Watanabe, T. Taniguchi, Z. Shi, T. Senthil, D. Goldhaber-Gordon, Y. Zhang, and F. Wang, Tunable correlated Chern insulator and ferromagnetism in a moiré superlattice, Nature (London) **579**, 56 (2020).

[18] Z. Hao, A. M. Zimmerman, P. Ledwith, E. Khalaf, D. H. Najafabadi, K. Watanabe, T. Taniguchi, A. Vishwanath, and P. Kim, Electric field–tunable superconductivity in alternating-twist magic-angle trilayer graphene, Science **371**, 1133 (2021).

[19] J. M. Park, Y. Cao, K. Watanabe, T. Taniguchi, and P. Jarillo-Herrero, Tunable strongly coupled superconductivity in magic-angle twisted trilayer graphene, Nature (London) **590**, 249 (2021).

[20] S. Chen, M. He, Y.-H. Zhang, V. Hsieh, Z. Fei, K. Watanabe, T. Taniguchi, D. H. Cobden, X. Xu, C. R. Dean, and M. Yankowitz, Electrically tunable correlated and topological states in twisted monolayer–bilayer graphene, Nat. Phys. **17**, 374 (2021).

[21] E. M. Alexeev, D. A. Ruiz-Tijerina, M. Danovich, M. J. Hamer, D. J. Terry, P. K. Nayak, S. Ahn, S. Pak, J. Lee, J. I. Sohn, M. R. Molas, M. Koperski, K. Watanabe, T. Taniguchi, K. S. Novoselov, R. V. Gorbachev, H. S. Shin, V. I. Fal'ko, and A. I. Tartakovskii, Resonantly hybridized excitons in moiré superlattices in van der Waals heterostructures, Nature (London) **567**, 81 (2019).

[22] K. Tran, G. Moody, F. Wu, X. Lu, J. Choi, K. Kim, A. Rai, D. A. Sanchez, J. Quan, A. Singh, J. Embley, A. Zepeda, M. Campbell, T. Autry, T. Taniguchi, K. Watanabe, N. Lu, S. K. Banerjee, K. L. Silverman, S. Kim, E. Tutuc, L. Yang, A. H. MacDonald, and X. Li, Evidence for moiré excitons in van der Waals heterostructures, Nature (London) **567**, 71 (2019).

[23] H. Yoo, R. Engelke, S. Carr, S. Fang, K. Zhang, P. Cazeaux, S. H. Sung, R. Hovden, A. W. Tsen, T. Taniguchi, K. Watanabe, G.-C. Yi, M. Kim, M. Luskin, E. B. Tadmor, E. Kaxiras, and P. Kim, Atomic and electronic reconstruction at the van der Waals interface in twisted bilayer graphene, Nat. Mater. **18**, 448 (2019).

[24] J. Quan, L. Linhart, M.-L. Lin, D. Lee, J. Zhu, C.-Y. Wang, W.-T. Hsu, J. Choi, J. Embley, C. Young, T. Taniguchi, K. Watanabe, C.-K. Shih, K. Lai, A. H. MacDonald, P.-H. Tan, F. Libisch, and X. Li, Phonon renormalization in reconstructed MoS_2 moiré superlattices, Nat. Mater. **20**, 1100 (2021).

[25] A. C. Gadelha, D. A. A. Ohlberg, C. Rabelo, E. G. S. Neto, T. L. Vasconcelos, J. L. Campos, J. S. Lemos, V. Ornelas, D. Miranda, R. Nadas, F. C. Santana, K. Watanabe, T. Taniguchi, B. van Troeye, M. Lamparski, V. Meunier, V.-H. Nguyen, D. Paszko, J.-C. Charlier, L. C. Campos, L. G. Cançado, G. Medeiros-Ribeiro, and A. Jorio, Localization of lattice dynamics in low-angle twisted bilayer graphene, Nature (London) **590**, 405 (2021).

[26] S. Chen, M. He, Y.-H. Zhang, V. Hsieh, Z. Fei, K. Watanabe, T. Taniguchi, D. H. Cobden, X. Xu, C. R. Dean, and M. Yankowitz, Electrically tunable correlated and topological states in twisted monolayer–bilayer graphene, Nat. Phys. **17**, 374 (2021).

[27] F. Wu, A. H. MacDonald, and I. Martin, Theory of Phonon-Mediated Superconductivity in Twisted Bilayer Graphene, Phys. Rev. Lett. **121**, 257001 (2018).

[28] Y. W. Choi and H. J. Choi, Strong electron-phonon coupling, electron-hole asymmetry, and nonadiabaticity in magic-angle twisted bilayer graphene, Phys. Rev. B **98**, 241412(R) (2018).

[29] T. J. Peltonen, R. Ojajärvi, and T. T. Heikkilä, Mean-field theory for superconductivity in twisted bilayer graphene, Phys. Rev. B **98**, 220504(R) (2018).

[30] B. Lian, Z. Wang, and B. A. Bernevig, Twisted Bilayer Graphene: A Phonon-Driven Superconductor, Phys. Rev. Lett. **122**, 257002 (2019).

[31] H. Polshyn, M. Yankowitz, S. Chen, Y. Zhang, K. Watanabe, T. Taniguchi, C. R. Dean, and A. F. Young, Large linear-in-temperature resistivity in twisted bilayer graphene, Nat. Phys. **15**, 1011 (2019).

[32] N. N. T. Nam and M. Koshino, Lattice relaxation and energy band modulation in twisted bilayer graphene, Phys. Rev. B **96**, 075311 (2017).

[33] L. Wirtz and A. Rubio, The phonon dispersion of graphite revisited, Solid State Commun. **131**, 141 (2004).

[34] A. N. Kolmogorov and V. H. Crespi, Registry-dependent interlayer potential for graphitic systems, Phys. Rev. B **71**, 235415 (2005).

[35] T. Nakanishi and T. Ando, Conductance of crossed carbon nanotubes, J. Phys. Soc. Jpn. **70**, 1647 (2001).

[36] P. Moon and M. Koshino, Energy spectrum and quantum Hall effect in twisted bilayer graphene, Phys. Rev. B **85**, 195458 (2012).

[37] See Supplemental Material at http://link.aps.org/supplemental/10.1103/PhysRevLett.127.167001 for (i) detailed descriptions of our atomistic calculation methods for relaxed atomic structures, phonon spectra, electronic structures, and electron-phonon matrix elements, and (ii) formulas for sublattice analysis of electron-phonon interaction, which includes Refs. [38–40].

[38] A. A. Maradudin and S. H. Vosko, Symmetry properties of the normal vibrations of a crystal, Rev. Mod. Phys. **40**, 1 (1968).

[39] A. Marek, V. Blum, R. Johanni, V. Havu, B. Lang, T. Auckenthaler, A. Heinecke, H.-J. Bungartz, and H. Lederer, The ELPA Library—Scalable Parallel Eigenvalue Solutions for Electronic Structure Theory and Computational Science, J. Condens. Matter Phys. **26**, 213201 (2014).

[40] P. E. Blöchl, O. Jepsen, and O. K. Andersen, Improved tetrahedron method for Brillouin-zone integrations, Phys. Rev. B **49**, 16223 (1994).

[41] S. Carr, C. Li, Z. Zhu, E. Kaxiras, S. Sachdev, and A. Kruchkov, Ultraheavy and Ultrarelativistic Dirac Quasiparticles in Sandwiched Graphenes, Nano Lett. **20**, 3030 (2020).

[42] Y. W. Choi and H. J. Choi, Intrinsic band gap and electrically tunable flat bands in twisted double bilayer graphene, Phys. Rev. B **100**, 201402(R) (2019).

[43] M. Angeli, E. Tosatti, and M. Fabrizio, Valley Jahn-Teller Effect in Twisted Bilayer Graphene Phys. Rev. X **9**, 041010 (2019).

[44] S. Carr, S. Fang, P. Jarillo-Herrero, and E. Kaxiras, Pressure dependence of the magic twist angle in graphene superlattices, Phys. Rev. B **98**, 085144 (2018).

[45] L. P. Gor'kov, Superconducting transition temperature: Interacting Fermi gas and phonon mechanisms in the nonadiabatic regime, Phys. Rev. B **93**, 054517 (2016).

[46] M. V. Sadovskii, Antiadiabatic phonons, coulomb pseudopotential, and superconductivity in Eliashberg-McMillan theory, JETP Lett. **109**, 166 (2019).

[47] J. M. Park, Y. Cao, K. Watanabe, T. Taniguchi, and P. Jarillo-Herrero, Flavour Hund's coupling, Chern gaps and charge diffusivity in moiré graphene, Nature (London) **592**, 43 (2021).

[48] Y. Cao, D. Rodan-Legrain, J. M. Park, N. F. Q. Yuan, K. Watanabe, T. Taniguchi, R. M. Fernandes, L. Fu, and P. Jarillo-Herrero, Nematicity and competing orders in superconducting magic-angle graphene, Science **372**, 264 (2021).

[49] B. Lian, Z.-D. Song, N. Regnault, D. K. Efetov, A. Yazdani, and B. A. Bernevig, Twisted bilayer graphene. IV. Exact insulator ground states and phase diagram, Phys. Rev. B **103**, 205414 (2021).

[50] Y. Saito, J. Ge, K. Watanabe, T. Taniguchi, and A. F. Young, Independent superconductors and correlated insulators in twisted bilayer graphene, Nat. Phys. **16**, 926 (2020).

[51] F. Guinea and N. R. Walet, Electrostatic effects, band distortions, and superconductivity in twisted graphene bilayers, Proc. Natl. Acad. Sci. U.S.A. **115**, 13174 (2018).

[52] C. Lewandowski, S. Nadj-Perge, and D. Chowdhury, Does filling-dependent band renormalization aid pairing in twisted bilayer graphene?, arXiv:2102.05661.

[53] T. Cea and F. Guinea, Coulomb interaction, phonons, and superconductivity in twisted bilayer graphene, Proc. Natl. Acad. Sci. U.S.A. **118**, e2107874118 (2021).

[54] M. S. Scheurer and R. Samajdar, Pairing in graphene-based moiré superlattices, Phys. Rev. Research **2**, 033062 (2020).

[55] R. Samajdar and M. S. Scheurer, Microscopic pairing mechanism, order parameter, and disorder sensitivity in moiré superlattices: Applications to twisted double-bilayer graphene, Phys. Rev. B **102**, 064501 (2020).